Clays and Clay Minerals, Vol. 44, No. 4, 492–500, 1996.

TEM AND X-RAY DIFFRACTION EVIDENCE FOR CRISTOBALITE AND TRIDYMITE STACKING SEQUENCES IN OPAL

JESSICA M. ELZEA[1] AND STEPHEN B. RICE[2]

[1] Thiele Kaolin Company, P.O. Box 1056, Sandersville, GA 31082
[2] McCrone Associates, 850 Pasquinelli Drive, Westmont, IL 60559

Abstract—In an attempt to resolve the structure of opal-CT and opal-C more precisely, 24 opal samples from bentonites, Fuller's Earths, zeolite tuffs, biogenic silicas and silicified kaolins have been analyzed by high resolution transmission electron microscopy (HRTEM) and X-ray diffraction (XRD). Results of this examination demonstrate that opal-C and opal-CT are part of a continuous series of intergrowths between end-member cristobalite and tridymite stacking sequences.

These findings are consistent with Flörke's (1955) interpretation of the most intense opal peak at ~4 Å as a combination of the (101) cristobalite and ($\bar{4}04$) tridymite peaks. The position and width of this peak are controlled by the relative volume of the two stacking types and the mean crystallite size. Direct evidence obtained by HRTEM provides data showing various stacking sequences in opals. Broadening due to crystallite size alone was determined by directly measuring crystallite size by TEM and comparing the measured size to the apparent size calculated using the Scherrer equation. XRD peak broadening is also described in terms of various contributions from structural disorder. The mean opal crystallite size ranges from 120 to 320 Å. For samples at either end of the size range, the crystallite size plays a larger role, relative to stacking disorder, in controlling peak broadening.

Key Words—Opal, Transmission Electron Microscopy, X-Ray Diffraction.

INTRODUCTION

The recognition that opal occurs widely within many rock types (Jones and Segnit 1971) and increasing interest of the application of silica diagenesis to inorganic paleothermometry (Rice et al. 1995) provide motivation to better characterize the structure of opal. Significant early contributions were made by Flörke (1955), who hypothesized on the basis of XRD that opals are disordered intergrowths of cristobalite and tridymite and by Jones et al. (1964), who determined that gem-quality opals are 3-dimensional arrays of amorphous silica spheres.

The structure of opal remains unresolved because these hydrated silica polymorphs produce XRD patterns that are characterized by broad, low intensity peaks and are therefore difficult to interpret. Some of the factors contributing to the XRD characteristics of opal minerals are water contents up to several percent, submicrometer crystallite sizes and stacking disorder within the silica framework. These same features limit the use of other techniques for obtaining unambiguous structural data. Spectroscopic techniques, including infrared spectroscopy (IR), ^{29}Si nuclear magnetic resonance (NMR) spectroscopy, Raman spectroscopy and X-ray absorption spectroscopy (XAS) have been applied to gain a clearer understanding of the amorphous nature and short-range ordering of opal (Langer and Flörke 1974; de Jong et al. 1987; Frölich 1989; Graetsch et al. 1990; Adams et al. 1991; Li et al. 1994; Rice et al. 1995). These spectroscopic methods do not depend on long-range order but instead measure short-range, molecular scale interactions such as stretching and bending of Si-O bonds. These methods provide useful structural information about crystalline and non-crystalline solids alike. Electron diffraction has also been applied to these minerals with limited success (Wilson et al. 1974). Instead of clarifying our understanding of the structure of opal, the data derived from these various analytical techniques have led to different and sometimes conflicting interpretations.

We have used XRD combined with HRTEM to gain insight into the structural nature of opals. We accomplish this by measuring the position of the main opal peak at ~4 Å and determining the relative contributions of small particle size and crystallographic disorder to the broadening of this peak. Inferences are made about the structure of opal from these data and direct imaging of the structures with TEM confirm the XRD model.

Structural Models for Opal

The following models are based primarily on XRD data supplemented by information derived from various spectroscopic techniques.

OPAL-A. The XRD pattern of opal-A is characterized by a single diffuse peak centered at approximately 4.1 Å (Figure 1). This mineral is interpreted as a highly disordered almost amorphous material similar to glass (Jones and Segnit 1971). Both IR and XAS data indicate that the short-range ordering of opal-A bears a

Copyright © 1996, The Clay Minerals Society

https://doi.org/10.1346/CCMN.1996.0440407 Published online by Cambridge University Press

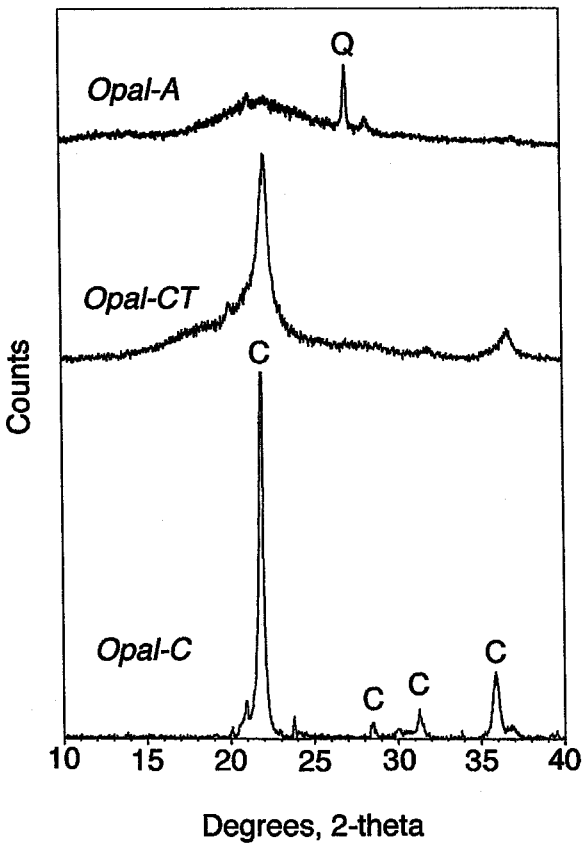


Figure 1. XRD scans for opal-A, opal-CT and opal-C. Quartz (Q) impurities are present within opal-A.

resemblance to cristobalite and tridymite. For example, the IR spectrum of opal-A from the Monterey Formation has an absorption band near 470 cm^{-1}, which is close to absorption bands assigned to Si-O bending modes for both tridymite and cristobalite (Rice et al. 1995). Similarly, the XAS spectrum of opal-A exhibits peaks reflecting crystal chemical parameters attributable to cristobalite (Li et al. 1994).

OPAL-CT. The diffraction pattern of opal-CT contains four moderately broad peaks that coincide closely with the positions of the four most intense α-cristobalite diffraction maxima (Figure 1). The most intense opal-CT reflection may occur anywhere from 4.07 to 4.10 Å and exhibits a range of peak widths (Elzea et al. 1994). The breadth and position of this peak are a consequence of the combination of two unresolved peaks, the α-cristobalite (101) and α-tridymite ($\bar{4}04$), as well as non-Bragg diffraction phenomena derived from the intergrowth of α-cristobalite and α-tridymite-like layers. In some cases, a secondary peak with a position close to the ($\bar{4}04$) α-tridymite line is observed on the high angle side of the main opal-CT reflection. However, none of the opals studied for this investigation exhibited this secondary peak. These data suggest that opal-CT has a cristobalite-like structure with varying degrees of stacking disorder leading to the appearance of tridymite reflections. Flörke (1955) proposed that this mineral is comprised of sheets of six-membered rings of silica tetrahedra stacked within random intergrowths of cristobalite (ABCABC . . .) and tridymite (A′ . . .) sequences where B is an A-layer shifted by a/3 and C is an A-layers shifted by −a/3, and A′ is an A-layer rotated 180°.

Wilson et al. (1974) offered another interpretation based on electron diffraction patterns and IR spectra from two opal samples. They concluded that opal-CT is essentially disordered tridymite. This conclusion is based partially on the similarity between the IR spectra of opal-CT and tridymite. Jones and Segnit (1971) also noted that the IR spectrum of opal-CT more closely resembles α-tridymite than α-cristobalite, but they argued that this observation is consistent with the one-dimensional stacking disorder model proposed by Flörke (1955). Rice et al. (1995) also observed a similarity between the spectroscopic signatures of opal-CT and tridymite.

A reinterpretation of the structure of opal-CT is given by de Jong et al. (1987), who combined XRD with ^{29}Si nuclear magnetic resonance spectroscopy to probe the structure of natural and synthetic opal. The NMR spectrum of opal-CT resembles amorphous silica much more than tridymite or cristobalite. This finding led the authors to conclude that long-range ordering of the oxygen array had taken place but that the Si atoms had not reached their equilibrium positions. They proposed three structural models for opal-CT that are consistent with both XRD and NMR data: 1) disordered cristobalite; 2) cristobalite with tridymite stacking sequences; or 3) tridymite with cristobalite stacking faults. Adams et al. (1991), using the same method, were unable to distinguish opal-CT from amorphous silica (opal-A).

Guthrie et al. (1995) used the WILDFIRE program to simulate XRD patterns for opal-CT and compared them to several natural opal-CT specimens. They found that a good match was obtained by modeling opal-CT as interstratified layers of cristobalite and tridymite and that some opal-CT is best modeled as a random interstratification and some opal-CT is best modeled as a partially ordered interstratification.

OPAL-C. Opal-C produces an XRD pattern that is almost identical to that of α-cristobalite in terms of peak position, number of reflections and peak intensity (Figure 1). However, both peak broadening and a slightly larger d-spacing provide indirect evidence for the presence of tridymite stacking disorder within this opal polymorph (Elzea et al. 1994). Opal-C has been interpreted as more ordered than opal-CT because it has sharper, more intense peaks.

https://doi.org/10.1346/CCMN.1996.0440407 Published online by Cambridge University Press

Table 1. Sample description and summary of XRD data for opal polymorphs.

Name/location	Rock type	~4 Å Peak		Sample #
		Position (Å)	Width (°2θ)	
Australia	Bentonite	4.043	0.263	AUST
Lovelock, NV	Bentonite	4.054	0.492	LNV
Upton, WY	Bentonite	4.040	0.332	UPWY
Mowry FM, WY	Bentonite	4.043	0.405	LMWY
Yell. C. Bed, WY	Bentonite	4.033	0.230	YCWY
Blue C. Bed, WY	Bentonite	4.038	0.269	BCWY
New Castle, WY	Bentonite	4.036	0.321	NCWY
Upper Bed, WY	Bentonite	4.043	0.355	UBWY
D-Bed, WY	Bentonite	4.044	0.249	DBWY
Texas	Bentonite	4.088	0.684	TEX
Chalk Hills, ID	Bentonite	4.070	0.778	CHID
Turkey	Bentonite	4.082	0.885	TRK
Mozambique	Bentonite	4.054	0.480	MOZ
Utah	Fuller's Earth	4.053	0.567	UTH
Porters Creek	Fuller's Earth	4.093	0.574	PC
Twiggs Fm, GA	Fuller's Earth	4.106	0.985	TCG
Monterey Fm, CA	Diatomaceous Earth	4.083	0.811	MCA
Leg 129	Porcellanite	4.102	0.757	L1291
Leg 129	Porcellanite	4.102	0.763	L1292
Wrens, GA	Silicified Limestone	4.108	0.654	WSL
Wrens, GA	Flint Kaolin	4.106	0.975	SNFC
Lovelock, NV	Zeolite Tuff	4.067	0.808	LZEO1
Lovelock, NV	Zeolite Tuff	4.077	—	LZEO2
Lovelock, NV	Zeolite Tuff	4.069	0.607	LZEO3

SAMPLES

Twenty-four samples of natural opal from bentonite, Fuller's earth, silicified kaolin, porcellanite, zeolitized tuff and diatomaceous sediments were analyzed by XRD (Table 1). Twelve of the 24 samples were further analyzed by HRTEM. In addition, XRD data were collected from 4 standards (Table 2). The amount of opal for this suite of samples is estimated to range from approximately 20% by volume in the bentonites and other clay deposits to 90% by volume for the purer diatomaceous earths. The opals examined in this study occur as secondary minerals deposited under a wide range of geochemical conditions and represent both volcanogenically and biogenically derived opal-CT and opal-C.

METHODS AND PROCEDURES

All samples were dried and pulverized to an average particle size of approximately 10 to 30 μm. No attempt was made to separate the opal from the matrix minerals because the presence of non-opal phases did not affect the quality of the XRD analysis for our purposes. Smectites often interfered with imaging the opal by TEM. Treatment to remove clays was tried for two specimens, but it only marginally improved imaging and introduced the potential for altering the opal.

Table 2. SiO_2 polymorph standards.

Mineral	Source
Tridymite (ty-27)	NIOSH
α-Cristobalite (cb-25)	NIOSH
α-Cristobalite (Gem Dugout)	Gem Dugout
α-Cristobalite (SRM 1879)	NIST

The powders were packed into sample holders and scanned on a Siemens D5000 X-ray diffractometer from 17.5 to 25 °2θ using CuKα radiation, a 0.01 °2θ step size and a 10 s per step data collection time. The Siemens peak fitting routine (FIT) was used to fit the patterns with either a Lorentzian or pseudo-Voigt function, and peak positions were determined from the fitted data using the position of the quartz (101) peak as an internal standard. Because the main opal peak cannot be resolved into two, it was modelled for fitting purposes as one peak. Peak width was calculated by measuring the width at half height (FWHM) and subtracting 0.0036 °2θ to correct for instrumental broadening. The corrected peak width was assumed to represent broadening caused by particle size and disorder.

Actual crystallite size was measured by TEM. The Scherrer equation was used to calculate FWHM expected for that average crystallite size. The amount of broadening attributable to disorder was calculated using the relation:

$$B_E^2 = B_S^2 + B_I^2 + B_D^2 \quad [1]$$

where: B_E = experimentally observed broadening (FWHM); B_S (measured by TEM) = broadening due to small particle size; B_I = broadening due to instrumental effects; and B_D = disorder broadening.

https://doi.org/10.1346/CCMN.1996.0440407 Published online by Cambridge University Press

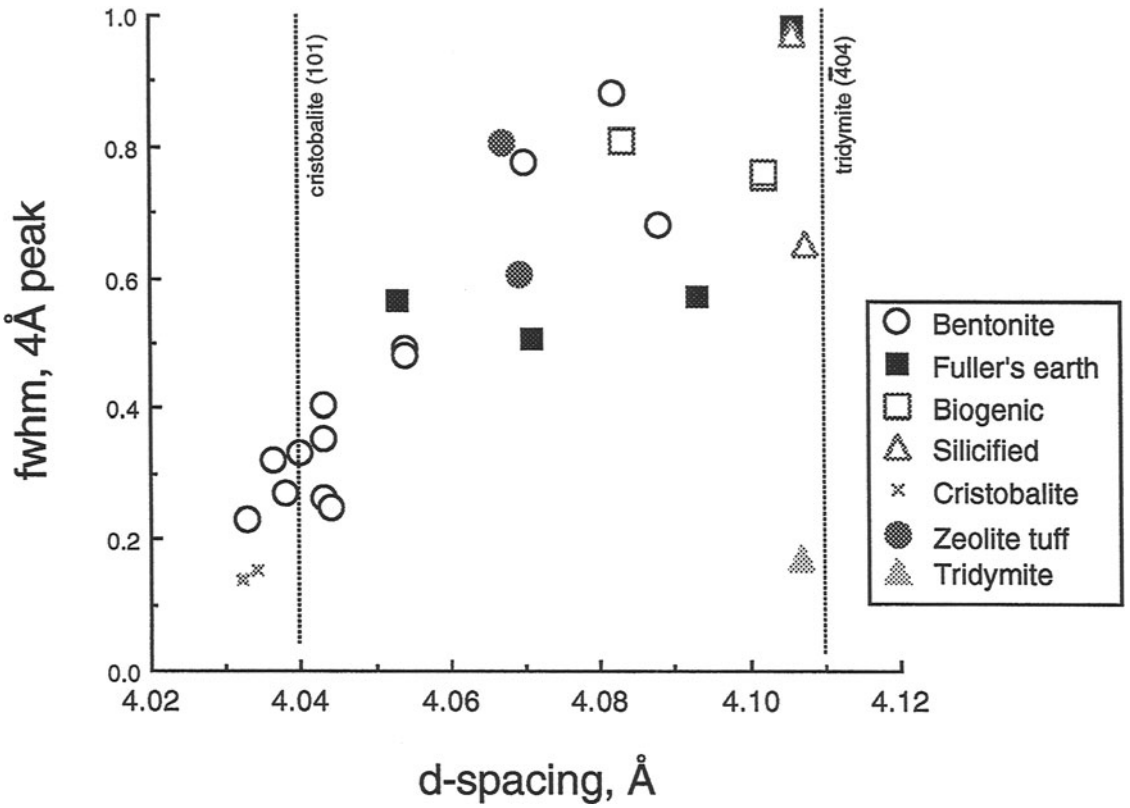


Figure 2. Width of the main opal peak (B_E) expressed as full-width at half maximum (FWHM) in °2θ. Synthetic cristobalite and tridymite reference materials are also plotted.

TEM samples were prepared by dispersing the powder in alcohol and depositing it on carbon coated copper TEM grids. Crystallite sizes were directly measured from negatives obtained on a JEOL 4000FX operated at 400 kV with an electron optical magnification of 200,000 ×. These conditions were chosen to minimize beam damage but yield a high enough resolution to allow observation of extremely fine details. Individual crystallites, viewed using conventional bright-field imaging and recognized based primarily upon phase and amplitude contrast, were measured for all samples except the zeolite tuffs. The longest dimension was recorded as the crystallite diameter. Because the opals are typically close to equidimensional, this provided a consistent way of measuring each sample. Mean crystallite sizes were determined from the measurement of approximately 550 crystallites per sample.

TEM was also used to obtain lattice images. For these observations an effort was made to minimize beam damage to the sample by dessicating the samples within the high vacuum of the microscope for several hours prior to examination and by limiting the electron dose during observation and image exposure. Image simulations were carried out using the MacTempas multislice program (Total Resolution, Berkeley, CA).

RESULTS AND DISCUSSION

The opals examined in this study exhibit a continuous range of spacings from approximately 4.03 to 4.11 Å and peak widths from 0.2 to 1 °2θ (Table 1). Opals with d-spacings closest to the position of the (101) cristobalite peak exhibit the narrowest diffraction maxima, and samples with maxima closest to the tridymite, preserve structural information $\bar{4}04$ peak position display the broadest diffraction maxima (Figure 2). According to the Jones and Segnit (1971) classification scheme, these opals fall into the opal-C and opal-CT categories. However, a precise division between these two polymorphs is not clear from our data. Instead, we suggest that opals are more accurately described as a continuous series extending from the cristobalite toward a hypothetical tridymite-like end-member phase.

Flörke's interpretation of the structure of these polymorphs predicts that opals with main maxima close to either the cristobalite or tridymite peak position will exhibit less broadening than will opals with peak positions intermediate between the two end-members. The small amount of broadening exhibited by the opals with peak positions close to that of cristobalite

https://doi.org/10.1346/CCMN.1996.0440407 Published online by Cambridge University Press

Table 3. Crystallite size data collected by TEM (mean size) and XRD (Scherrer size).

Sample #	Mean size, Å	Scherrer size, Å	B_S	B_D	$\%B_S$	$\%B_D$
AUST	320	342	0.284	0.000	100	0
LNV	297	183	0.306	0.385	44	56
UPWY	311	271	0.292	0.158	65	35
MOZ	279	187	0.317	0.360	47	53
TCG	117	91	0.767	0.618	55	45
MCA	262	111	0.349	0.737	32	68
L1291	279	119	0.326	0.683	32	68
L1292	257	118	0.350	0.678	34	66
WSL	250	137	0.352	0.551	39	61
SNFC	134	95	0.671	0.707	49	51
LZEO1	>1000	111	0.009	0.808	1	99
LZEO3	>1000	148	0.009	0.607	1	99

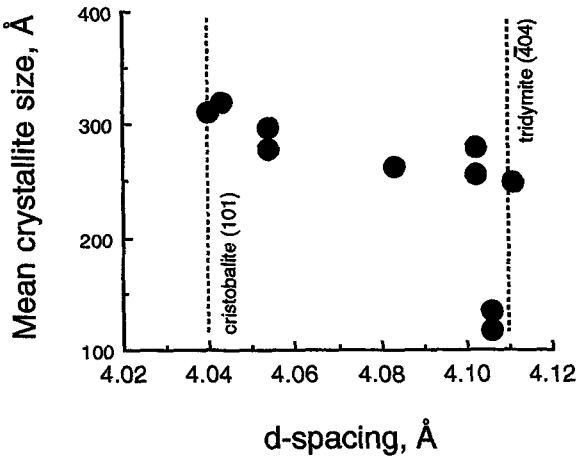


Figure 3. Mean crystallite sizes as measured by TEM for 10 opal specimens plotted against the d-spacing of the main opal peak measured by XRD.

are consistent with this model. But, the samples with maxima close to the tridymite peak show more peak broadening than would be expected from the presence of a small amount of cristobalite domains. This peak broadening may be due to particle size. However, random interstratification of the two layer types cannot be discounted as a contributor.

To test the hypothesis that crystallite size influences peak broadening, the broadening caused by small crystallite size alone was determined by directly measuring crystallite size with the TEM and solving the Scherrer equation for peak width. An apparent crystallite size was also calculated from the XRD data and compared to that obtained by TEM. According to our TEM measurements, the opals in all samples, except for LZEO1 and LZEO3, have mean crystallite sizes ranging from approximately 120 to 320 Å as compared to 91 to 342 Å calculated from XRD patterns (Table 3). Crystallite sizes calculated from XRD patterns are, except for one sample, smaller than crystallite sizes measured by TEM. This discrepancy between calculated and measured crystallite sizes suggests that there are contributions to peak broadening other than crystallite size.

Opals with 4 Å peak d-spacings closest to the tridymite ($\bar{4}04$) peak position tend to have the smallest mean crystallite sizes as measured by TEM (Figure 3), suggesting that the relative contribution to broadening by crystallite size alone varies. Peak broadening caused by crystallite size (B_S) ranges from approximately 0.3 to 0.7 °2θ, whereas peak broadening caused by disorder (B_D) ranges from approximately 0.0 to 0.8 °2θ (Table 3). For the majority of samples, crystallite size (B_S) accounts for 32 to 50% of the total broadening (Table 3). The percentage of peak broadening attributable to disorder (B_D) varies from 0 to 99% (Figure 4).

The relative impact of disorder on line broadening is small for samples that exhibit d-spacings close to the cristobalite end-member (Figure 4). Conversely, line broadening due to disorder is greatest for samples with d-spacings intermediate to the cristobalite (101) and tridymite ($\bar{4}04$) peak positions. These observations support a structural model for opal-CT that is consistent with the one originally proposed by Flörke (1955). Opal-CT consists of intergrowths of cristobalite and tridymite domains that lead to varying amounts of line broadening depending upon the relative volumes of cristobalite and tridymite domains. The frequency of stacking changes also influence the broadening by reducing the effective domain sizes and contributing to the non-Bragg components recorded within the diffraction patterns. According to this model, opals with a proportionally higher volume of cristobalite or tridymite layers will have more narrow peaks that shift toward the position of the most abundant end-member. This model further predicts that opals with similar volumes of cristobalite and tridymite layers will have broader peaks that fall between the cristobalite and tridymite peak positions. Thus, the model predicts that B_D versus the position of the main opal peak will be an inverted parabola.

The only inconsistency between the proposed model and the data plotted in Figure 5 is the asymmetry of the curve close to the tridymite ($\bar{4}04$) peak position. The model predicts less disorder broadening close to the position of this peak than is observed. There may be several explanations for this higher than expected degree of disorder broadening. The presence of cristobalite domains could be a major factor. There also may be several types of disorder. For example, Al substitution for Si and/or cation substitution, variable OH structural positions, or variable H_2O content within the tridymitic phase. Errors associated with either the TEM crystallite size measurements or the calculation of the peak width from the XRD data are also possible. These more tridymitic opals tend to have much broader, less intense peaks than the more cristobalitic end-

https://doi.org/10.1346/CCMN.1996.0440407 Published online by Cambridge University Press

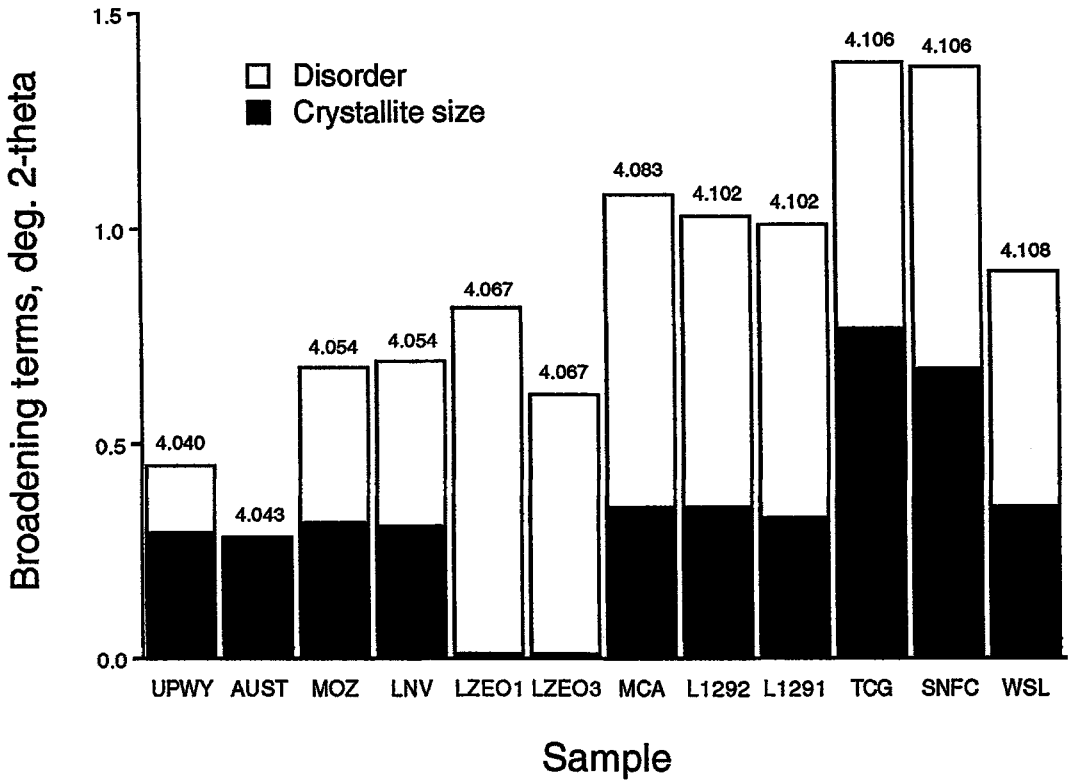


Figure 4. Relative contribution of crystallite size and disorder (B_D) to the total breadth (B_E) measured for 12 opal samples. See text for explanation of how these values were determined. Values over bars are d-spacings.

members, leading to errors in the FWHM measurement and increased error during the peak fitting. Finally, the calculated Scherrer size relates to the size of the coherent diffraction domain rather than the actual size of the crystallite. For example, consider a 100 Å crystal that has a very thin cristobalite layer in the middle. The effective size, as seen by diffraction, is a ≤50 Å domain. Thus, the size broadening could exceed predicted size measurements alone for specimens having predominantly tridymite domains with only minor cristobalite layers or other stacking faults.

To obtain more direct evidence for the presence of two layer types in opal-CT, HRTEM images were recorded for several samples. These images are interpreted in terms of idealized coherent stackings of trigonal silica nets and give direct evidence that opal-CT is comprised of interlayered cristobalite and tridymite stacking sequences.

Figure 6a shows a high resolution micrograph of a portion of an opal crystallite from the Wyoming bentonite. To improve the quality of the experimental image, fast Fourier transform (FFT) filtering was performed to remove non-periodic components resulting from the carbon support, radiation damage and shot noise. A mask filter was then applied to the FFT and an inverse transform was carried out (Figure 6b). Caution was taken to avoid imposing periodicities on regions containing none to begin with. The 4 Å interlayer spacing and the 72° angle between the intersecting sets of lattice fringes agree with the ABCABC . . . stacking sequence of cristobalite as demonstrated by agreement with the simulated image of the (100) projection of α-cristobalite (Figure 6c). This is the most commonly observed periodic image for the opal-C samples.

The opal-C samples also contain noncrystalline material. It is not known to what extent this is genuinely non-crystalline as opposed to crystallites whose long-range order has been disrupted by beam damage. The XRD patterns, even of opal-C, consistently contain a broad, low intensity hump suggestive of a non-crystalline component such as opal-A. The TEM data were ambiguous.

High resolution electron microscope images were obtained for several samples with main peak positions greater than 4.04 Å: Monterey opal-CT (MCA, 4.083 Å), silicified kaolin (SNFC, 4.106 Å) and silicified limestone (WSL, 4.108 Å). In contrast to the opal-C from bentonite, these all included cristobalite stacking but also showed substantial departure from the ideal cristobalite stacking in many images. Examples are presented here for opals from the silicified kaolin.

https://doi.org/10.1346/CCMN.1996.0440407 Published online by Cambridge University Press

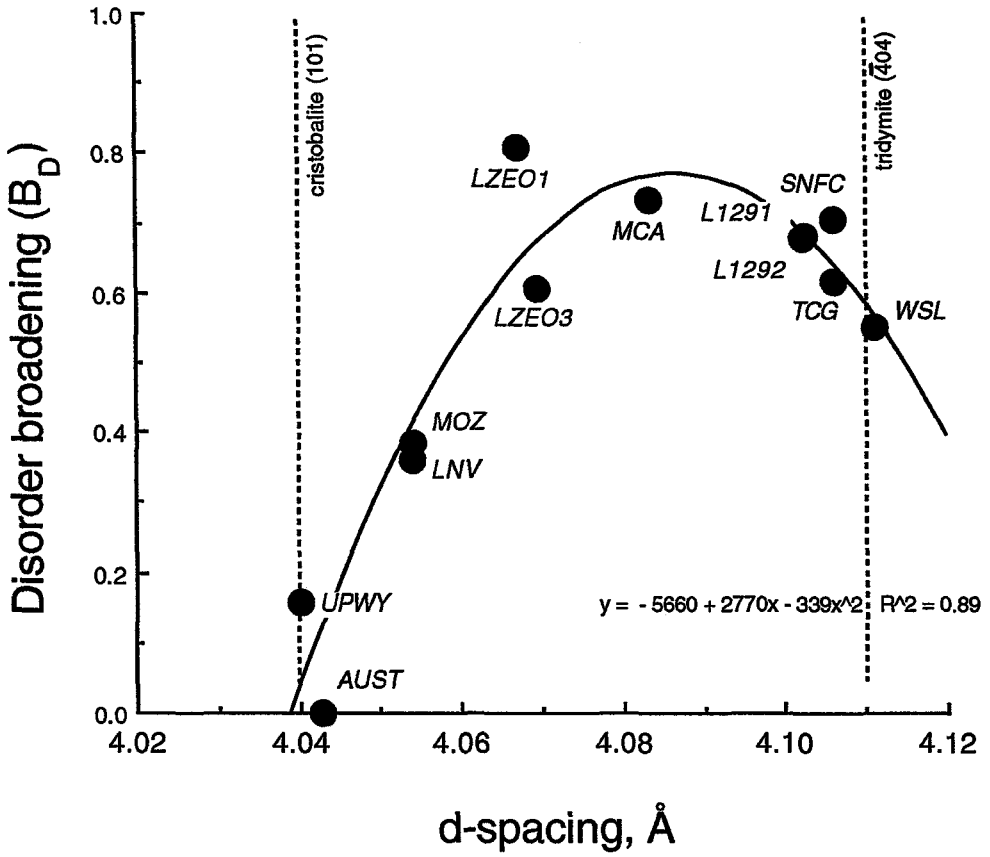


Figure 5. Contribution of disorder broadening (B_D) plotted against d-spacing of main opal peak.

Figure 7a shows an experimental lattice image of a portion of an opal crystallite characterized by cristobalite stacking at the top, tridymite stacking in the middle, and cristobalite at the bottom. The Fourier filtered version is shown in Figure 7b, and the stacking schematically is depicted in Figure 7c. Image simulation for the tridymite (110) projection (Figure 7b, inset) demonstrates agreement between calculated and experimental images. The schematic version applies mainly to the right side of the image. A close look at the tridymite region (Figure 7b) reveals a reversal in the direction of the vertical "zig-zag" pattern near the middle produced by adjacent tridymite layers. On the right side of the image, the tridymite stacking order is AA′A and on the left side stacking order changes to A′AA′. There is a dislocation defect approximately

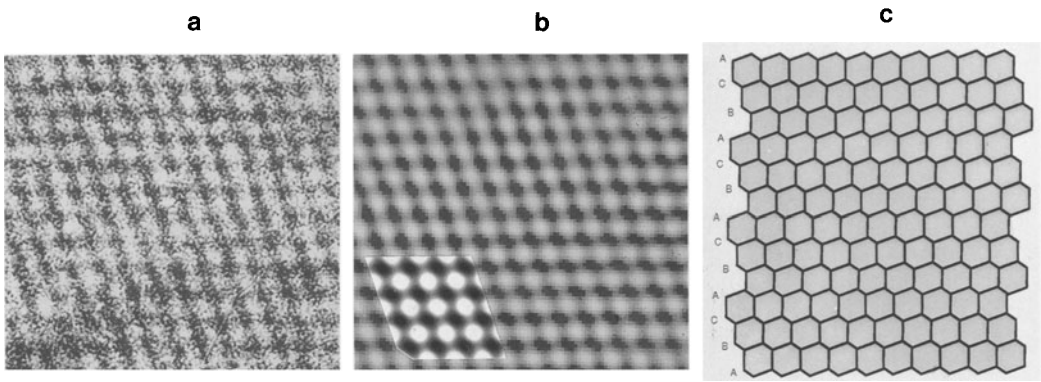


Figure 6. a) TEM lattice image of opal crystallite within Wyoming bentonite (UPWY); b) Fourier filtered version of image in (a); c) structure drawing of cristobalite stacking for comparison. Inset in (b) is a simulation of the (100) projection of α-cristobalite.

https://doi.org/10.1346/CCMN.1996.0440407 Published online by Cambridge University Press

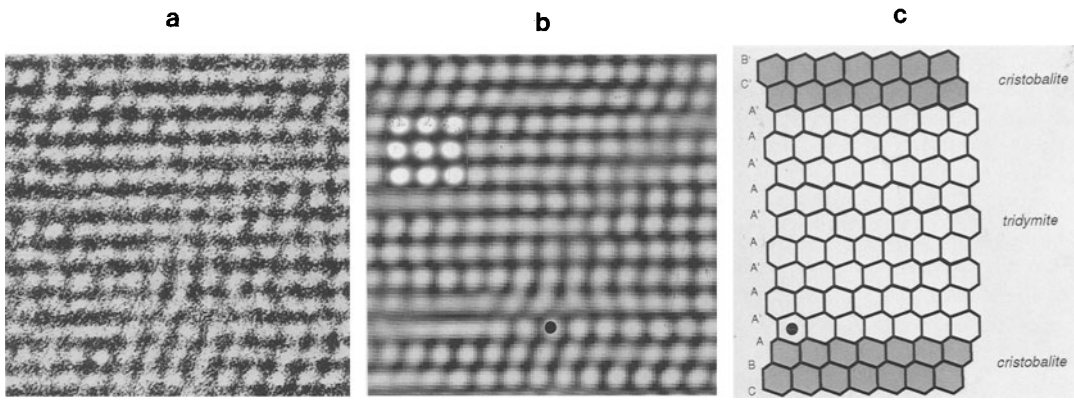


Figure 7. a) Lattice image of opal crystallite in silicified kaolin (SNFC); b) cristobalite stacking is evident in the top and bottom of the Fourier filtered image; c) schematic drawing for stacking observed on the right half of the image. Inset in (b) is a simulation of the (110) projection of high-tridymite.

where this reversal meets the cristobalite stacking sequence. Its termination is indicated by a dot at the bottom central portion of the image. Other disturbances, such as in the lower left, are difficult to interpret because they probably include differences through the thickness of projection.

Figure 8a shows an experimental image of an opal crystallite whose cristobalite stacking is interrupted by several planar boundaries. Fourier filtering is vital for correct interpretation. What appear from the experimental image to be four or five twin boundaries are indicated to be two minimum tridymite units (AA′A-type repeats) occurring between cristobalite sequences, one of which has a twin boundary. It is obvious how the presence of tridymite domains would strongly affect the diffraction behavior, but there is also a potential impact if opal crystallites were to be polysynthetically twinned. The schematic drawing in Figure 8c shows how cristobalite twins relate to one another across the twin boundary. The stacking of adjacent hexagonal nets on either side of the twin plane is identical to the fundamental increment for ideal tridymite. As the twinning density increases, accompanied by a cristobalite domain size decrease, the specimen will appear more like a disordered tridymite.

It is difficult to estimate how much of each stacking type is present within rock samples on the basis of a few lattice images. Furthermore, based on opal-C images and intragrain comparisons from the opal-CT images, cristobalite stacking is better preserved during imaging than the tridymite stacking. However, in spite of these caveats, we infer from our survey of opal-CT samples that substantial cristobalite stacking occurs, even for opal d-spacings of approximately 4.1 Å. There is probably sufficient disorder of this type to create XRD peak broadening that is measurable. This is in contrast to the opal-C end of the series, in which negligible tridymite stacking occurs. The broadening expected from a 40 to 80 Å domain thickness, a reasonable estimate for the silicified kaolin, could also be invoked to explain much of the measured B_D. Other types of disorder due to factors such as Al substitution

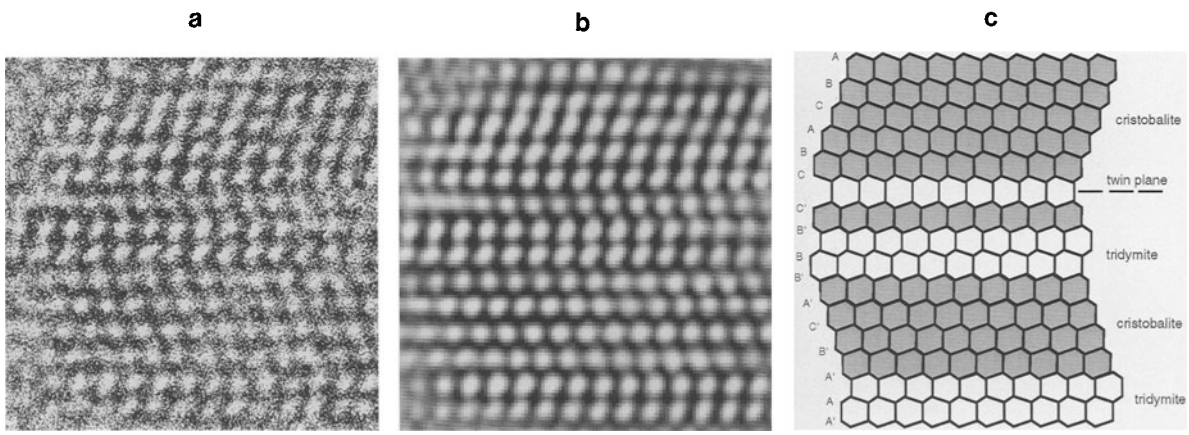


Figure 8. a) Lattice image of opal crystallite in silicified kaolin (SNFC) showing intergrown cristobalite and tridymite; b) Fourier filtered image; c) structure drawing of mixed cristobalite and tridymite stacking including a twin plane.

https://doi.org/10.1346/CCMN.1996.0440407 Published online by Cambridge University Press

for Si and associated cation substitution required to maintain charge balance, impurities and water contents, would not manifest themselves in images. Disorder defects such as shown in Figure 7b are also candidates for modifying the main diffraction maxima, but estimates of their frequency are speculative. Although tridymite stacking is very common, perhaps even prevalent for opals whose d-spacings are near 4.1 Å, we have not yet encountered what could be legitimately called opal-T.

SUMMARY

We have shown that the opal polymorphs represent a continuous series of disordered intergrowths between end-member cristobalite and tridymite stacking sequences. By using mean crystallite sizes directly measured from TEM images, we were able to distinguish the XRD line broadening due to crystallite size from that due to structural disorder. The resulting data show that opals with 4 Å peaks close to the position of the cristobalite (101) peak have minimum disorder broadening and opals with 4 Å peaks in between the positions of the cristobalite (101) and tridymite ($\bar{4}04$) peak positions exhibit the maximum disorder broadening. The opals with X-ray maxima closest to the tridymite ($\bar{4}04$) peak, exhibit a greater degree of disorder broadening than expected from XRD and size-corrected data. At the tridymite end, it is likely that a combination of factors such as cristobalite stacking and twinning, domain size considerations and other types of disorder, are responsible for the broadening.

ACKNOWLEDGMENTS

The authors wish to thank I.E. Odom, W.F. Moll, Jr. and W.J. Miles for providing some of the samples. The authors also gratefully acknowledge J. Barabe for assistance with the figures and M. Rice for assistance with particle size measurements. We also would like to thank G. Guthrie for his very helpful review of the manuscript.

REFERENCES

Adams SJ, Hawkes GE, Curzon EH. 1991. A solid state ^{29}Si nuclear magnetic resonance study of opal and other hydrous silicas. Am Miner 76:1863–1871.

de Jong BHW, van Hoek SJ, Veeman WS, Manson DV. 1987. X-ray diffraction and ^{29}Si magic-angle spinning NMR of opals: Incoherent long- and short-range order in opal-CT. Am Miner 72:1195–1203.

Elzea JM, Odom IE, Miles WJ. 1994. Distinguishing well ordered opal-CT and opal-C from high temperature cristobalite by x-ray diffraction. Analytica Chim Acta 286: 107–116.

Flörke OW. 1955. Zur frage des "hoch"-cristobalit in opalen, bentoniten und gläsern. Neues Jahrbuch für Mineralogie Monatshefte 217–233.

Frölich F. 1989. Deep-sea biogenic silica: new structural and analytical data from infrared analysis—geological implications. Terra Nova 1:267–273.

Graetsch H, Mosset A, Gies H. 1990. XRD and ^{29}Si MAS-NMR study on some non-crystalline silica minerals. J Noncrystal Sol 119:173–180.

Guthrie GO, Jr., Bish DL, Reynolds RC, Jr. 1995. Modeling the X-ray diffraction patterns of opal. Am Miner 80:869–872.

Jones JB, Sanders JV, Segnit ER. 1964. Structure of opal. Nature 204:990–991.

Jones JB, Segnit ER. 1971. The nature of opal I. Nomenclature and constituent phases. J Geol Soc Aust 18:57–68.

Langer K, Flörke OW. 1974. Near infrared absorption spectra (4000–9000 cm^{-1}) of opals and the role of "water" in these SiO_2nH_2O minerals. Fortschrift der Miner 52:17–51.

Li D, Bancroft GM, Kasrai M, Fleet ME, Secco RA, Feng XH, Tan KH, Yang BX. 1994. X-ray absorption spectroscopy of silicon dioxide (SiO_2) polymorphs: The structural characterization of opal. Am Miner 79:622–632.

Rice SB, Freund H, Clouse JA, Fleissner TG, Isaacs CM. 1995. Application of Fourier transform infrared spectroscopy to silica diagenesis: the opal-A to opal-CT transformation, A. Sedimentary Processes. J Sedimen Res A65: 639–647.

Wilson MJ, Russell JD, Tate JM. 1974. A new interpretation of the structure of disordered α-cristobalite. Contributions to Mineral & Petrol 47:1–6.

(Received 6 January 1995; accepted 3 October 1995; Ms. 2604)

https://doi.org/10.1346/CCMN.1996.0440407 Published online by Cambridge University Press